 CMES, vol.83, no.3, pp.249-273, 2012

Large Rotation Analyses of Plate/Shell Structures Based on the Primal Variational Principle and a Fully Nonlinear Theory in the Updated Lagrangian Co-Rotational Reference Frame

Y.C. Cai[1] **and S.N. Atluri**[2]

Abstract: This paper presents a very simple finite element method for geometrically nonlinear large rotation analyses of plate/shell structures comprising of thin members. A fully nonlinear theory of deformation is employed in the updated Lagrangian reference frame of each plate element, to account for bending, stretching and torsion of each element. An assumed displacement approach, based on the Discrete Kirchhoff Theory (DKT) over each element, is employed to derive an explicit expression for the (18x18) *symmetric* tangent stiffness matrix of the plate element in the co-rotational reference frame. The finite rotation of the updated Lagrangian reference frame relative to a globally fixed Cartesian frame, is simply determined from the finite displacement vectors of the nodes of the 3-node element in the global reference frame. The element employed here is a 3-node plate element with 6 degrees of freedom per node, including 1 drilling degree of freedom and 5 degrees of freedom [3 displacements, and the derivatives of the transverse displacement around two independent axes]. The present (18×18) symmetric tangent stiffness matrices of the plate, based on the primal variational principle and the fully nonlinear plate theory in the updated Lagrangian reference frame, are much simpler than those of many others in the literature for large rotation/deformation analysis of plate/shell structures. Numerical examples demonstrate the accuracy and robustness of the present method.

Keywords: large deformation, thin plate/shell, Discrete Kirchhoff Theory (DKT), updated Lagrangian formulation, Primal principle.

[1] Key Laboratory of Geotechnical and Underground Engineering of Ministry of Education, Department of Geotechnical Engineering, Tongji University, Shanghai 200092, P.R.China.
[2] Center for Aerospace Research & Education, University of California, Irvine

1 Introduction

Exact and efficient nonlinear large deformation analyses of space structures have significance in diverse engineering applications, such as civil and aerospace engineering. Over the past 3 decades, many different methods were developed by numerous researchers for the linear and nonlinear analyses of 3D plate/shell structures. For example, Kang, Zhang and Wang (2009), Kulikov and Plotnikova (2008), Nguyen-Van, Mai-Duy and Tran-Cong (2007) developed several displacement plate-/shell elements based on the Kirchhoff or Mindlin theories. Chin and Zhang (1994), Choo, Choi and Lee (2010), Huang, Shenoy and Atluri (1994), Maunder and Moitinho (2005) proposed some hybrid plate element based on assumed strain distributions or hybrid principles. Iura and Atluri (1992) employed the drilling degrees of freedom in plate/shell elements to avoid the problem of singularity in the stiffness matrix. Iura and Atluri (2003), Gal and Levy (2006), Rajendran and Narasimhan (2006), Wu, Chiu and Wang (2008) overviewed some progress of the plate analyses. Albuquerque and Aliabadi (2008), Baiz and Aliabadi (2006), Fedelinski and Gorski (2006) developed the boundary element formulations for the analyses of plates or shells. Atluri and his co-workers (Atluri 1980; Atluri and Cazzani 1994; Atluri 2005) extensively studied the large rotations in plates and shells, and attendant variational principles involving the rotation tensor as a direct variable. These diverse theories and methods of the plate/shell have now been widely applied to a variety of problems.

Although a large number of different efforts have been made, some inherent difficulties related to the linear/nonlinear analyses of 3D plate/shell structures still need to be further overcome. The objective of this paper is to provide an essentially elementary engineering treatment of plates and shells undergoing large deformations and rotations without resorting to the highly mathematical tools of differential geometry, and group –theoretical treatment of finite rotations, as in most of the prior literature. This paper presents a simple finite element method for large deformation/large rotation analyses of plate/shell structures comprising of thin members. A fully nonlinear theory of deformation is employed in the updated Lagrangian reference frame of each plate element, to account for bending, stretching, and torsion of each element. An assumed displacement approach, based on the Discrete Kirchhoff Theory (DKT) over each element, is employed to derive an explicit expression for the (18x18) *symmetric* tangent stiffness matrix of the plate element in the updated Lagrangian reference frame. Numerical examples demonstrate the accuracy and robustness of the present method.

2 A fully nonlinear theory for a plate undergoing moderately large deformations in the updated Lagrangian reference frame

We consider a fixed global reference frame with axes $\bar{x}_i\,(i=1,2,3)$ and base vectors $\bar{\mathbf{e}}_i$. The plate in its undeformed state, with local coordinates $\tilde{x}_i\,(i=1,2,3)$ and base vectors $\tilde{\mathbf{e}}_i$, is located arbitrarily in space, as shown in Fig.1. The current configuration of the plate, after arbitrarily large deformations, is also shown in Fig.1. The local coordinates in the reference frame in the current configuration are x_i and the base vectors are $\mathbf{e}_i\,(i=1,2,3)$.

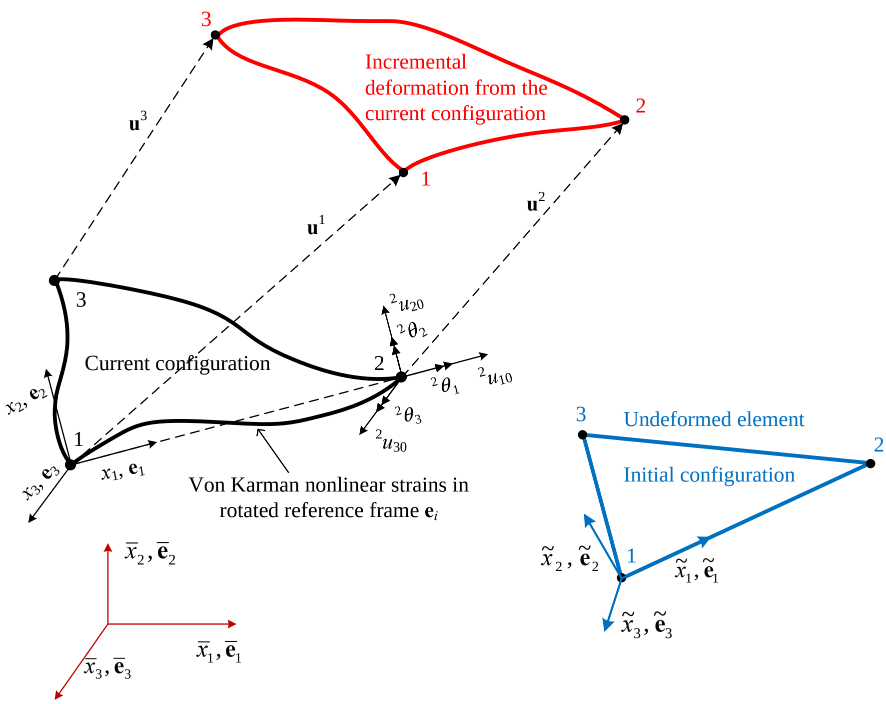

Figure 1: Updated Lagrangian reference frame for a plate element

As shown in Fig.2, we consider the large deformations of a typical thin plate. A fully nonlinear theory (retaining all the nonlinear terms in the relations between the incremental strains and incremental displacements) of deformation is assumed for the continued deformation from the current configuration, in the updated Lagrangian frame of reference $\mathbf{e}_i\,(i=1,2,3)$ in the local coordinates $x_i\,(i=1,2,3)$. If h is the characteristic thickness of the thin plate, and $u_i\,(x_j)$ are the displacements of the plate from the current configuration in the $\mathbf{e}_i$ directions, the precise

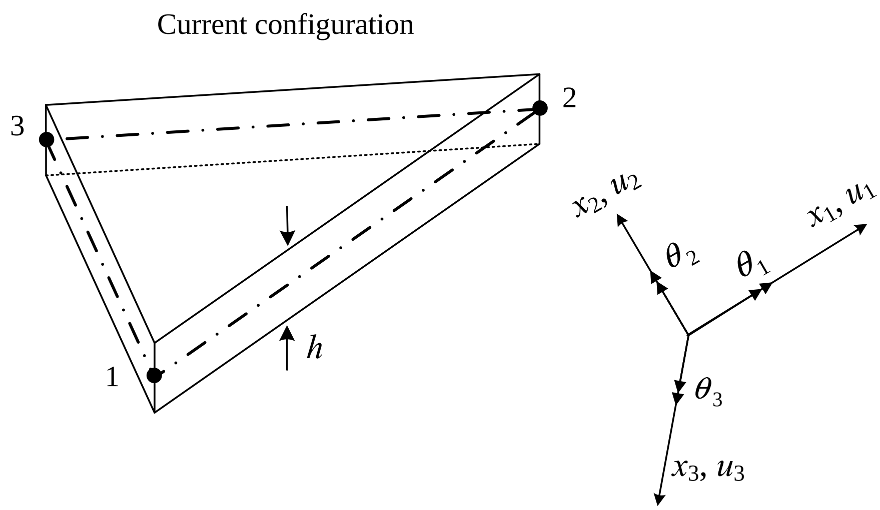

Figure 2: Large deformation analysis model of a plate element

assumptions governing the continued deformations from the current configuration are ($\alpha = 1,2; \beta = 1,2,3$)

1. $\frac{h}{L} \ll 1$ (the plate is thin);

2. $u_3/h \sim \mathrm{O}(1)$;

3. $\left(\frac{\partial u_3}{\partial x_\alpha}\right) \ll 1$;

4. $u_\alpha/h \ll 1$;

5. $\left(\frac{\partial u_\alpha}{\partial x_\beta}\right)^2$ and $\left(\frac{\partial u_3}{\partial x_\alpha}\right)^2$ are all retained as nonlinear terms in the co-rotational frame of reference;

6. All strains $E_{\alpha\beta} \ll 1$ [where $E_{\alpha\beta}$ are strains from the current configuration, in the x_α coordinates];

7. The material is linear. For elastic-plastic material, the rate relation is bi-linear.

Thus, the generally 3-dimensional displacement state in the $\mathbf{e}_i$ system is simplified to be of the type

$$
\begin{aligned}
u_1 &= u_{10}(x_\alpha) - x_3 \frac{\partial u_3}{\partial x_1} \\
u_2 &= u_{20}(x_\alpha) - x_3 \frac{\partial u_3}{\partial x_2}
\end{aligned}
\tag{1}
$$

where

$$
\begin{aligned}
u_3 &= u_{30}(x_1, x_2) \\
u_{10} &= u_{10}(x_1, x_2) \\
u_{20} &= u_{20}(x_1, x_2)
\end{aligned}
\tag{2}
$$

2.1 Strain-displacement relations

Considering the complete nonlinearities in the rotated reference frame $\mathbf{e}_i(x_i)$, we can write the Green-Lagrange strain-displacement relations in the updated Lagrangian co-rotational frame $\mathbf{e}_i$ in Fig.1 as (Cai, Paik and Atluri 2010):

$$
\mathbf{E} = \mathbf{E}^L + \mathbf{E}^N \tag{3}
$$

where

$$
\begin{aligned}
\mathbf{E}^L &= \begin{bmatrix} E_{11}^L & E_{22}^L & E_{12}^L & E_{21}^L \end{bmatrix}^T \\
&= \begin{bmatrix} u_{10,1} - x_3 u_{30,11} & u_{20,2} - x_3 u_{30,22} & u_{10,2} - x_3 u_{30,12} + \theta_3 & u_{20,1} - x_3 u_{30,12} - \theta_3 \end{bmatrix}^T
\end{aligned}
\tag{4}
$$

$$
\mathbf{E}^N = \begin{bmatrix} E_{11}^N & E_{22}^N & E_{12}^N & E_{21}^N \end{bmatrix}^T \tag{5}
$$

where $,i$ denotes a differentiation with respect to x_i, $\theta_3 = \frac{1}{2}(u_{20,1} - u_{10,2})$ are the drilling degrees of freedom, $2E_{11}^N = u_{10,1}^2 + u_{20,1}^2 + u_{30,1}^2$, $2E_{22}^N = u_{10,2}^2 + u_{20,2}^2 + u_{30,2}^2$, and $2E_{12}^N = 2E_{21}^N = u_{10,1}u_{10,2} + u_{20,1}u_{20,2} + u_{30,1}u_{30,2}$.

2.2 Stress-Strain relations

The stress-measure conjugate to these strains is the second Piola-Kirchhoff stress tensor $\mathbf{S}^1\ \left[S_{ij}^1\right]$.

We assume a state of plane-stress to derive the stresses from strains in a thin plate as

$$
\mathbf{S}^1 = \tilde{\mathbf{D}}\left(\boldsymbol{\varepsilon}^L + \boldsymbol{\varepsilon}^N\right) = \mathbf{S}^{1\mathrm{L}} + \mathbf{S}^{1\mathrm{N}} \tag{6}
$$

where

$$\tilde{\mathbf{D}} = \frac{E}{1-\nu^2}\begin{bmatrix} 1 & \nu & 0 & 0 \\ \nu & 1 & 0 & 0 \\ 0 & 0 & 1-\nu & 0 \\ 0 & 0 & 0 & 1-\nu \end{bmatrix} \tag{7}$$

where E is the elastic modulus; ν is the Poisson ratio.

2.3 Generalized stresses

If the mid-surface of the plate is taken as the reference plane in the co-rotational updated Lagrangian reference frame, the generalized forces of the plate in Fig.2 can be defined as

$$\boldsymbol{\sigma} = \mathbf{D}\boldsymbol{\varepsilon} \tag{8}$$

where $\boldsymbol{\sigma}$ are the element generalized stresses, $\boldsymbol{\varepsilon}$ are the element generalized strains, and

$$\boldsymbol{\sigma} = \begin{Bmatrix} \sigma_1 \\ \sigma_2 \\ \sigma_3 \\ \sigma_4 \\ \sigma_5 \\ \sigma_6 \\ \sigma_7 \end{Bmatrix} = \begin{Bmatrix} N_{11} \\ N_{22} \\ N_{12} \\ N_{21} \\ M_{11} \\ M_{22} \\ M_{12} \end{Bmatrix} \tag{9}$$

$$\boldsymbol{\varepsilon} = \begin{Bmatrix} \varepsilon_1 \\ \varepsilon_2 \\ \varepsilon_3 \\ \varepsilon_4 \\ \varepsilon_5 \\ \varepsilon_6 \\ \varepsilon_7 \end{Bmatrix} = \boldsymbol{\varepsilon}^L + \boldsymbol{\varepsilon}^N = \begin{Bmatrix} u_{10,1} \\ u_{20,2} \\ u_{10,2} + \theta_3 \\ u_{20,1} - \theta_3 \\ -u_{30,11} \\ -u_{30,22} \\ -2u_{30,12} \end{Bmatrix} + \frac{1}{2}\begin{Bmatrix} u_{10,1}^2 + u_{20,1}^2 + u_{30,1}^2 \\ u_{10,2}^2 + u_{20,2}^2 + u_{30,2}^2 \\ u_{10,1}u_{10,2} + u_{20,1}u_{20,2} + u_{30,1}u_{30,2} \\ u_{10,1}u_{10,2} + u_{20,1}u_{20,2} + u_{30,1}u_{30,2} \\ 0 \\ 0 \\ 0 \end{Bmatrix} \tag{10}$$

$$\mathbf{D} = \begin{bmatrix} C & \nu C & 0 & 0 & 0 & 0 & 0 \\ \nu C & C & 0 & 0 & 0 & 0 & 0 \\ 0 & 0 & C_1 & 0 & 0 & 0 & 0 \\ 0 & 0 & 0 & C_1 & 0 & 0 & 0 \\ 0 & 0 & 0 & 0 & D & \nu D & 0 \\ 0 & 0 & 0 & 0 & \nu D & D & 0 \\ 0 & 0 & 0 & 0 & 0 & 0 & D_1 \end{bmatrix} \tag{11}$$

where $C = \frac{Eh}{1-\nu^2}$, $D = \frac{Eh^3}{12(1-\nu^2)}$, $C_1 = (1-\nu)C$ and $D_1 = (1-\nu)D/2$.
If we denote $\theta_1 = u_{30,1}$ and $\theta_2 = u_{30,2}$, Eq. (10) can be rewritten as

$$\boldsymbol{\varepsilon}^L = \mathbf{LU} = \begin{bmatrix} u_{10,1} & u_{20,2} & u_{10,2}+\theta_3 & u_{20,1}-\theta_3 & -\theta_{1,1} & -\theta_{2,2} & -\theta_{1,2}-\theta_{2,1} \end{bmatrix}^T \tag{12}$$

$$\boldsymbol{\varepsilon}^N = \frac{1}{2}\mathbf{A}_\theta \mathbf{U}_\theta \tag{13}$$

where

$$\mathbf{L} = \begin{bmatrix} \partial/\partial x_1 & 0 & 0 & 0 & 0 & 0 \\ 0 & \partial/\partial x_2 & 0 & 0 & 0 & 0 \\ \partial/\partial x_2 & 0 & 0 & 0 & 0 & 1 \\ 0 & \partial/\partial x_1 & 0 & 0 & 0 & -1 \\ 0 & 0 & 0 & -\partial/\partial x_1 & 0 & 0 \\ 0 & 0 & 0 & 0 & -\partial/\partial x_2 & 0 \\ 0 & 0 & 0 & -\partial/\partial x_2 & -\partial/\partial x_1 & 0 \end{bmatrix} \tag{14}$$

$$\mathbf{A}_\theta = \begin{bmatrix} u_{10,1} & u_{20,1} & \theta_1 & 0 & 0 & 0 \\ 0 & 0 & 0 & u_{10,2} & u_{20,2} & \theta_2 \\ u_{10,2}/2 & u_{20,2}/2 & \theta_2/2 & u_{10,1}/2 & u_{20,1}/2 & \theta_1/2 \\ u_{10,2}/2 & u_{20,2}/2 & \theta_2/2 & u_{10,1}/2 & u_{20,1}/2 & \theta_1/2 \\ 0 & 0 & 0 & 0 & 0 & 0 \\ 0 & 0 & 0 & 0 & 0 & 0 \\ 0 & 0 & 0 & 0 & 0 & 0 \end{bmatrix} \tag{15}$$

$$\mathbf{U} = \begin{bmatrix} u_{10} & u_{20} & u_{30} & \theta_1 & \theta_2 & \theta_3 \end{bmatrix}^T \tag{16}$$

$$\mathbf{U}_\theta = \begin{bmatrix} u_{10,1} & u_{20,1} & \theta_1 & u_{10,2} & u_{20,2} & \theta_2 \end{bmatrix}^T \tag{17}$$

3 Interpolation functions

As shown in Fig.2, the plate element has three nodes with 6 degrees of freedom per node. By defining the following DKT displacements functions

$$\begin{aligned} \theta_1 &= \sum_{i=1}^{3} (R_i w_i + R_{xi}\theta_{1i} + R_{yi}\theta_{2i}) \\ \theta_2 &= \sum_{i=1}^{3} (H_i w_i + H_{xi}\theta_{1i} + H_{yi}\theta_{2i}) \end{aligned} \tag{18}$$

where

$$R_1 = 1.5\left(m_6N_6/l_6 - m_4N_4/l_4\right), \quad R_2 = 1.5\left(m_4N_4/l_4 - m_5N_5/l_5\right),$$

$$R_3 = 1.5\left(m_5N_5/l_5 - m_6N_6/l_6\right),$$
$$R_{x1} = N_1 + N_4\left(0.5n_4^2 - 0.25m_4^2\right) + N_6\left(0.5n_6^2 - 0.25m_6^2\right),$$
$$R_{x2} = N_2 + N_4\left(0.5n_4^2 - 0.25m_4^2\right) + N_5\left(0.5n_5^2 - 0.25m_5^2\right),$$
$$R_{x3} = N_3 + N_5\left(0.5n_5^2 - 0.25m_5^2\right) + N_6\left(0.5n_6^2 - 0.25m_6^2\right),$$
$$R_{y1} = -0.75\left(m_4n_4N_4 + m_6n_6N_6\right), \quad R_{y2} = -0.75\left(m_4n_4N_4 + m_5n_5N_5\right),$$
$$R_{y3} = -0.75\left(m_5n_5N_5 + m_6n_6N_6\right);$$

$$H_1 = 1.5\left(n_6N_6/l_6 - n_4N_4/l_4\right), \quad H_2 = 1.5\left(n_4N_4/l_4 - n_5N_5/l_5\right),$$

$$H_3 = 1.5\left(n_5N_5/l_5 - n_6N_6/l_6\right),$$
$$H_{x1} = R_{y1}, \quad H_{x2} = R_{y2}, \quad H_{x3} = R_{y3},$$
$$H_{y1} = N_1 + N_4\left(0.5m_4^2 - 0.25n_4^2\right) + N_6\left(0.5m_6^2 - 0.25n_6^2\right),$$
$$H_{y2} = N_2 + N_4\left(0.5m_4^2 - 0.25n_4^2\right) + N_5\left(0.5m_5^2 - 0.25n_5^2\right),$$
and

$$H_{y3} = N_3 + N_5\left(0.5m_5^2 - 0.25n_5^2\right) + N_6\left(0.5m_6^2 - 0.25n_6^2\right);$$

l_k is the length of side ij ($i = 1,2,3$ and $j = 2,3,1$ when $k = 4,5,6$); $m_k = \cos\alpha_k$ and $n_k = \sin\alpha_k$ ($k = 4,5,6$) where α_k is defined in Fig.3;

$$\begin{aligned} &N_j = (2L_j - 1)\,L_j \;\; (j = 1,2,3) \\ &N_4 = 4L_1L_2, N_5 = 4L_2L_3, N_6 = 4L_3L_1 \end{aligned} \tag{19}$$

L_i are the area coordinates of the three-node triangular plate elements and can be expressed as

$$L_i = \frac{1}{2A}\left(a_i + b_ix_1 + c_ix_2\right) \tag{20}$$

$$a_i = x_1^jx_2^m - x_1^mx_2^j,\; b_i = x_2^j - x_2^m,\; c_i = -x_1^j + x_1^m \tag{21}$$

where $i = 1,2,3$; $j = 2,3,1$; $m = 3,1,2$, and A is the area of the triangular element, we can approximate the displacement function in each plate element by

$$\mathbf{U} = \mathbf{N}\hat{\mathbf{a}} = \begin{bmatrix} \mathbf{N}_1 & \mathbf{N}_2 & \mathbf{N}_2 \end{bmatrix} \begin{Bmatrix} \hat{\mathbf{a}}_1 \\ \hat{\mathbf{a}}_2 \\ \hat{\mathbf{a}}_3 \end{Bmatrix} \tag{22}$$

where the displacement function **U** is defined in Eq.(16), the displacement vectors of node i in the updated Lagrangian frame $\mathbf{e}_i$ of Fig.2 are:

$$\hat{\mathbf{a}}^i = \begin{bmatrix} u_{10}^i & u_{20}^i & u_{30}^i & \theta_1^i & \theta_2^i & \theta_3^i \end{bmatrix}^T \ [i = 1,2,3] \tag{23}$$

$$\mathbf{N}_i = \begin{bmatrix} L_i & 0 & 0 & 0 & 0 & 0 \\ 0 & L_i & 0 & 0 & 0 & 0 \\ 0 & 0 & L_i & 0 & 0 & 0 \\ 0 & 0 & R_i & R_{xi} & R_{yi} & 0 \\ 0 & 0 & H_i & H_{xi} & H_{yi} & 0 \\ 0 & 0 & 0 & 0 & 0 & L_i \end{bmatrix} \ [i = 1,2,3] \tag{24}$$

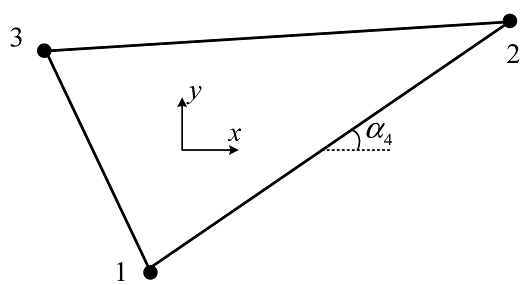

Figure 3: Triangular plate element

From Eqs.(12), (13) and (22), we obtain

$$\boldsymbol{\varepsilon} = \boldsymbol{\varepsilon}^L + \boldsymbol{\varepsilon}^N = \left(\mathbf{B}^L + \hat{\mathbf{B}}^N\right) \hat{\mathbf{a}} \tag{25}$$

where

$$\mathbf{B}^L = \begin{bmatrix} \mathbf{B}_1^L & \mathbf{B}_2^L & \mathbf{B}_3^L \end{bmatrix} \tag{26}$$

$$\mathbf{B}_i^L = \begin{bmatrix} L_{i,1} & 0 & 0 & 0 & 0 & 0 \\ 0 & L_{i,2} & 0 & 0 & 0 & 0 \\ L_{i,2} & 0 & 0 & 0 & 0 & L_i \\ 0 & L_{i,1} & 0 & 0 & 0 & -L_i \\ 0 & 0 & -R_{i,1} & -R_{xi,1} & -R_{yi,1} & 0 \\ 0 & 0 & -H_{i,2} & -H_{xi,2} & -H_{yi,2} & 0 \\ 0 & 0 & -R_{i,2}-H_{i,1} & -R_{xi,2}-H_{xi,1} & -R_{yi,2}-H_{yi,1} & 0 \end{bmatrix} \tag{27}$$

$$\hat{\mathbf{B}}^N = \mathbf{A}_\theta \mathbf{G}/2 \tag{28}$$

where

$$\mathbf{G} = \begin{bmatrix} \mathbf{G}_1 & \mathbf{G}_2 & \mathbf{G}_3 \end{bmatrix} \tag{29}$$

$$\mathbf{G}_i = \begin{bmatrix} L_{i,1} & 0 & 0 & 0 & 0 & 0 \\ 0 & L_{i,1} & 0 & 0 & 0 & 0 \\ 0 & 0 & R_i & R_{xi} & R_{yi} & 0 \\ L_{i,2} & 0 & 0 & 0 & 0 & 0 \\ 0 & L_{i,2} & 0 & 0 & 0 & 0 \\ 0 & 0 & H_i & H_{xi} & H_{yi} & 0 \end{bmatrix} \tag{30}$$

and thus

$$\delta(\boldsymbol{\varepsilon}) = \left(\mathbf{B}^L + 2\hat{\mathbf{B}}^N\right)\delta\hat{\mathbf{a}} = \left(\mathbf{B}^L + \mathbf{B}^N\right)\delta(\mathbf{a}) = \mathbf{B}\delta\hat{\mathbf{a}} \tag{31}$$

4 Updated Lagrangian formulation in the co-rotational reference frame $\mathbf{e}_i$

If τ_{ij}^0 are the initial Cauchy stresses in the updated Lagrangian co-rotational frame $\mathbf{e}_i$ of Fig.1, and S_{ij}^1 are the additional (incremental) second Piola-Kirchhoff stresses in the same updated Lagrangian co-rotational frame with axes $\mathbf{e}_i$, then the static equations of linear momentum balance and the stress boundary conditions in the frame $\mathbf{e}_i$ are given by

$$\frac{\partial}{\partial x_i}\left[\left(S_{ik}^1 + \tau_{ik}^0\right)\left(\delta_{jk} + \frac{\partial u_j}{\partial x_k}\right)\right] + b_j = 0 \tag{32}$$

$$\left(S_{ik}^1 + \tau_{ik}^0\right)\left(\delta_{jk} + \frac{\partial u_j}{\partial x_k}\right) n_i - f_j = 0 \tag{33}$$

where b_j are the body forces per unit volume in the current reference state, and f_j are the given boundary loads.

By letting $S_{ik} = S^1_{ik} + \tau^0_{ik}$, the equivalent weak form of the above equations can be written as

$$\int_V \left\{ \frac{\partial}{\partial x_i} \left[S_{ik} \left(\delta_{jk} + \frac{\partial u_j}{\partial x_k} \right) \right] + b_j \right\} \delta u_j dV - \int_{S_\sigma} \left[S_{ik} \left(\delta_{jk} + \frac{\partial u_j}{\partial x_k} \right) n_i - f_j \right] \delta u_j dS = 0 \tag{34}$$

where δu_j are the test functions.

By integrating by parts the first item of the left side, the above equation can be written as

$$\int_V -S_{ik} \left(\delta_{jk} + \frac{\partial u_j}{\partial x_k} \right) \delta u_{j,\,i} dV + \int_V b_j \delta u_j dV + \int_{S_\sigma} f_j \delta u_j dS = 0 \tag{35}$$

From Eq.(6) we may write

$$S^1_{ik} = S^{1L}_{ik} + S^{1\mathrm{N}}_{ik} \tag{36}$$

Then the first item of Eq.(35) becomes

$$\begin{aligned} S_{ik} \left(\delta_{jk} + u_{j,k} \right) \delta u_{j,i} &= \left(\tau^0_{ij} + \tau^0_{ik} u_{j,k} + S^{1L}_{ij} + S^{1\mathrm{N}}_{ij} + S^1_{ik} u_{j,k} \right) \delta u_{j,i} \\ &= S^{1L}_{ij} \delta \varepsilon^L_{ij} + \tau^0_{ik} \delta \left(\frac{1}{2} u_{j,k} u_{j,i} \right) + \left(\tau^0_{ij} + S^{1\mathrm{N}}_{ij} + S^1_{ik} u_{j,k} \right) \delta u_{j,i} \end{aligned} \tag{37}$$

By using Eq.(5), Eq.(35) may be written as

$$\int_V \left(S^{1L}_{ij} \delta \varepsilon^L_{ij} + \tau^0_{ij} \delta \varepsilon^N_{ij} \right) dV = \int_V b_j \delta u_j dV + \int_{S_\sigma} f_j \delta u_j dS - \int_V \left(\tau^0_{ij} + S^{1\mathrm{N}}_{ij} + S^1_{ik} u_{j,k} \right) \delta \varepsilon^L_{ij} dV \tag{38}$$

The terms on the right hand side are ‘correction’ terms in a Newton-Rapson type iterative approach. Carrying out the integration over the cross sectional of each plate, and using Eqs.(3) to (31), Eq.(38) can be easily shown to reduce to:

$$\begin{aligned} &\sum_e \left[\delta \hat{\mathbf{a}}^T \int_A \left(\mathbf{B}^L \right)^T \mathbf{D} \mathbf{B}^L dA \; \hat{\mathbf{a}} + \delta \hat{\mathbf{a}}^T \int_A \left(\mathbf{B}^N \right)^T \boldsymbol{\sigma}^0 dA \right] = \\ &\sum_e \left[\delta \hat{\mathbf{a}}^T \hat{\mathbf{F}}^1 - \delta \hat{\mathbf{a}}^T \int_A \left(\mathbf{B}^L \right)^T \left(\boldsymbol{\sigma}^0 + \boldsymbol{\sigma}^{1\mathrm{N}} \right) dA \; - \delta \hat{\mathbf{a}}^T \int_A \left(\mathbf{B}^N \right)^T \boldsymbol{\sigma}^1 dA \right] \end{aligned} \tag{39}$$

where $\hat{\mathbf{F}}^1 = \int\limits_V \mathbf{N^T b}^* \, dV + \int\limits_{S_\sigma} \mathbf{N^T f}^* \, dS$ is the external equivalent nodal force.

If we neglect the nonlinear items in Eq.(39) for the convenience of solving the non-linear equation, Eq.(39) can be rewritten as

$$\sum_e \left[\delta \hat{\mathbf{a}}^T \left(\hat{\mathbf{K}}^L + \hat{\mathbf{K}}^S\right) \, \hat{\mathbf{a}}\right] = \sum_e \left[\delta \hat{\mathbf{a}}^T \left(\hat{\mathbf{F}}^1 - \hat{\mathbf{F}}^S\right) \, \right] \tag{40}$$

where $\hat{\mathbf{K}} = \hat{\mathbf{K}}^L + \hat{\mathbf{K}}^S$ is the *symmetric tangent stiffness matrix* of the plate element,

$$\hat{\mathbf{K}}^L = \int_A \left(\mathbf{B}^L\right)^T \mathbf{D}\mathbf{B}^L dA \quad \text{[linear part]} \tag{41}$$

$$\hat{\mathbf{K}}^S = \int_A \left(\mathbf{B}^N\right)^T \boldsymbol{\sigma}^0 dA = \int_A \mathbf{G}^T \boldsymbol{\sigma}_\theta^0 \mathbf{G} dA \quad \text{[nonlinear part]} \tag{42}$$

$$\hat{\mathbf{F}}^S = \int_A \left(\mathbf{B}^L\right)^T \boldsymbol{\sigma}^0 dA \tag{43}$$

where the element generalized stresses are updated by using $\boldsymbol{\sigma} = \boldsymbol{\sigma}^0 + \boldsymbol{\sigma}^{1\mathrm{L}}$,

$$\boldsymbol{\sigma}_\theta^0 = \begin{bmatrix} N_{11}^0 \mathbf{I} & \frac{N_{12}^0 + N_{21}^0}{2} \mathbf{I} \\ \frac{N_{12}^0 + N_{21}^0}{2} \mathbf{I} & N_{22}^0 \mathbf{I} \end{bmatrix} \tag{44}$$

$$\mathbf{I} = \begin{bmatrix} 1 & 0 & 0 \\ 0 & 1 & 0 \\ 0 & 0 & 1 \end{bmatrix} \tag{45}$$

The *tangent* stiffness matrix $\hat{\mathbf{K}} = \hat{\mathbf{K}}^L + \hat{\mathbf{K}}^S$ is a 18×18 *symmetric matrix*, and can be explicitly expressed with the coordinates of the nodes of the triangular element, by using the Eqs. (11), (26), (28) and (44).

It is clear from the above procedures, that the explicit expression and the numerical implementation of the present (18×18) symmetric tangent stiffness matrices of the plate in the co-rotational reference frame, based on the primal theory, are much simpler than those based on Reissner variational principle (Cai, Paik and Atluri 2010) and many others in the literature for large rotation/deformation analysis of built-up plate/shell structures

5 Transformation between deformation dependent co-rotational local $[\mathbf{e}_i]$, and the global $[\bar{\mathbf{e}}_i]$ frames of reference

As shown in Fig.1, $\bar{x}_i\,(i = 1,2,3)$ are the global coordinates with unit basis vectors $\bar{\mathbf{e}}_i$. By letting x_i and $\mathbf{e}_i$ be the co-rotational reference coordinates for the deformed plate element, the basis vectors $\mathbf{e}_i$ are chosen such that

$$\begin{aligned}
&\mathbf{e}_1 = \left(x_1^{12}\bar{\mathbf{e}}_1 + x_2^{12}\bar{\mathbf{e}}_2 + x_3^{12}\bar{\mathbf{e}}_3\right)/l^{12} = \tilde{a}_1\bar{\mathbf{e}}_1 + \tilde{a}_2\bar{\mathbf{e}}_2 + \tilde{a}_3\bar{\mathbf{e}}_3 \\
&\mathbf{e}_3 = \tilde{c}_1\bar{\mathbf{e}}_1 + \tilde{c}_2\bar{\mathbf{e}}_2 + \tilde{c}_3\bar{\mathbf{e}}_3 \\
&\mathbf{e}_2 = \mathbf{e}_3 \times \mathbf{e}_1
\end{aligned} \tag{46}$$

where $x_i^{jk} = x_i^j - x_i^k,\; l^{jk} = \left[\left(x_1^{jk}\right)^2 + \left(x_2^{jk}\right)^2 + \left(x_3^{jk}\right)^2\right]^{\frac{1}{2}}$,

$$\tilde{b}_1 = \frac{x_1^{13}}{l^{13}}, \tilde{b}_2 = \frac{x_2^{13}}{l^{13}}, \tilde{b}_3 = \frac{x_3^{13}}{l^{13}} \tag{47}$$

$$\tilde{c}_1 = \frac{\tilde{a}_2\tilde{b}_3 - \tilde{a}_3\tilde{b}_2}{l^c}, \tilde{c}_2 = \frac{\tilde{a}_3\tilde{b}_1 - \tilde{a}_1\tilde{b}_3}{l^c}, \tilde{c}_3 = \frac{\tilde{a}_1\tilde{b}_2 - \tilde{a}_2\tilde{b}_1}{l^c} \tag{48}$$

and

$$l^c = \left[\left(\tilde{a}_2\tilde{b}_3 - \tilde{a}_3\tilde{b}_2\right)^2 + \left(\tilde{a}_3\tilde{b}_1 - \tilde{a}_1\tilde{b}_3\right)^2 + \left(\tilde{a}_1\tilde{b}_2 - \tilde{a}_2\tilde{b}_1\right)^2\right]^{\frac{1}{2}} \tag{49}$$

Then $\mathbf{e}_i$ and $\bar{\mathbf{e}}_i$ have the following relations:

$$\begin{Bmatrix} \mathbf{e}_1 \\ \mathbf{e}_2 \\ \mathbf{e}_3 \end{Bmatrix} = \begin{bmatrix} \tilde{a}_1 & \tilde{a}_2 & \tilde{a}_3 \\ \tilde{d}_1 & \tilde{d}_2 & \tilde{d}_3 \\ \tilde{c}_1 & \tilde{c}_2 & \tilde{c}_3 \end{bmatrix} \begin{Bmatrix} \bar{\mathbf{e}}_1 \\ \bar{\mathbf{e}}_2 \\ \bar{\mathbf{e}}_3 \end{Bmatrix} \tag{50}$$

where

$$\tilde{d}_1 = \tilde{c}_2\tilde{a}_3 - \tilde{c}_3\tilde{a}_2, \tilde{d}_2 = \tilde{c}_3\tilde{a}_1 - \tilde{c}_1\tilde{a}_3, \tilde{d}_3 = \tilde{c}_1\tilde{a}_2 - \tilde{c}_2\tilde{a}_1 \tag{51}$$

$$\boldsymbol{\lambda}_0 = \begin{bmatrix} \tilde{a}_1 & \tilde{a}_2 & \tilde{a}_3 \\ \tilde{d}_1 & \tilde{d}_2 & \tilde{d}_3 \\ \tilde{c}_1 & \tilde{c}_2 & \tilde{c}_3 \end{bmatrix} \tag{52}$$

Thus, the transformation matrix $\boldsymbol{\lambda}$ for the plate element, between the 18 generalized coordinates in the co-rotational reference frame $\mathbf{e}_i$, and the corresponding 18 coordinates in the global Cartesian reference frame $\bar{\mathbf{e}}_i$, is given by

$$\boldsymbol{\lambda} = \begin{bmatrix} \boldsymbol{\lambda}_0 & 0 & 0 & 0 & 0 & 0 \\ 0 & \boldsymbol{\lambda}_0 & 0 & 0 & 0 & 0 \\ 0 & 0 & \boldsymbol{\lambda}_0 & 0 & 0 & 0 \\ 0 & 0 & 0 & \boldsymbol{\lambda}_0 & 0 & 0 \\ 0 & 0 & 0 & 0 & \boldsymbol{\lambda}_0 & 0 \\ 0 & 0 & 0 & 0 & 0 & \boldsymbol{\lambda}_0 \end{bmatrix} \tag{53}$$

Then the element matrices are transformed to the global coordinate system using

$$\bar{\mathbf{a}} = \boldsymbol{\lambda}^T \mathbf{a} \tag{54}$$

$$\bar{\mathbf{K}} = \boldsymbol{\lambda}^T \mathbf{K} \boldsymbol{\lambda} \tag{55}$$

$$\bar{\mathbf{F}} = \boldsymbol{\lambda}^T \mathbf{F} \tag{56}$$

where $\bar{\mathbf{a}}, \bar{\mathbf{K}}, \bar{\mathbf{F}}$ are respectively the generalized nodal displacements, element tangent stiffness matrix and generalized nodal forces, in the global coordinates system. The Newton-Raphson method is used to solve the nonlinear equation of the plate in this implementation.

6 Numerical examples

6.1 Buckling of the thin plate

The (18×18) tangent stiffness matrix for a plate in space should be capable of predicting buckling under compressive axial loads, when such an axial load interacts with the transverse displacement in the plate. We consider the plate with two types of boundary conditions as shown in Figs.4a and 4b. Assume that the thickness of the plate is $h = 0.01$, and $a = b = D = 1$. The buckling loads of the plate obtained by the present method using different numbers of elements are shown in Tab.1. It is seen that the buckling load predicted by the present method agrees well with the analytical solution (buckling load is $P_{cr} = k\pi^2 D/b^2$, where $k = 4$ for Fig.4a and $k = 1.7$ for Fig.4b).

6.2 A simply supported or clamped square plate

A simply supported or clamped square plate loaded by a central point load p or a uniform load q is considered for linear elastic analysis. The side length and the thickness of the square plate are l and h. The results listed in Tab.2 and Tab.3 indicate the good accuracy and convergence rate of the present elements. Numerical results also indicate that, although the primal methods are used, the displacement solutions of the example are not always convergence from "BELOW" for the DKT-type approach.

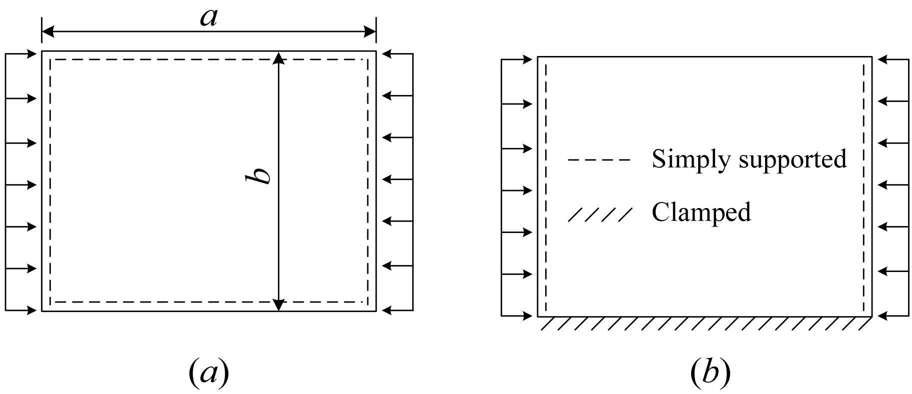

Figure 4: Model of the plate subject to an axial force

Table 1: Buckling load of the plate

Mesh	Fig.4a		Fig.4b	
	Present method	Exact	Present method	Exact
4×4	39.7001	39.4784	17.0938	16.7783
8×8	39.4956		16.8422	
16×16	39.4787		16.7807	

Table 2: Central deflection for a square plate clamped along all four boundaries

Mesh	Uniform load $\left(w_c \times ql^4/100D\right)$	Point load $\left(w_c \times pl^2/100D\right)$
2×2	0.1212	0.6342
4×4	0.1257	0.5905
8×8	0.1263	0.5706
16×16	0.1265	0.5640
Exact	0.1260	0.5600

6.3 Geometrically nonlinear analysis of a clamped square plate subjected to a uniform load

The geometrically nonlinear analysis of a clamped plate under uniform load q is studied (Cui, Liu, Li, Zhao, Nguyen, and Sun 2008). The side length and the thickness of the square plate are $l = 100mm$ and $h = 1mm$. The material properties are $E = 2.1e06N/mm^2$ and $\nu = 0.316$. The analytic central solution of the plate is

Table 3: Central deflection for a square plate simply supported along all four boundaries

Mesh	Uniform load $\left(w_c \times ql^4/100D\right)$	Point load $\left(w_c \times pl^2/100D\right)$
2×2	0.3673	1.2820
4×4	0.3972	1.1993
8×8	0.4040	1.1719
16×16	0.4057	1.1635
Exact	0.4062	1.1600

given by chia (1980):

$$\left(\frac{w_0}{h}\right)^3 + 0.2522\frac{w_0}{h} = 0.0001333\frac{ql^4}{Dh} \tag{57}$$

where $w_c = 2.5223w_0$.

The whole plate is modeled and the central deflection w_c of the plate for different meshes is shown in Tab.4. It is observed that the results of the present method converge quickly to the analytic solution.

Table 4: The central deflection of a clamped square plate subjected to a uniform load

Mesh	q				
	0.5	1.3	2.1	3.4	5.5
4×4	0.340689	0.736689	0.999181	1.294422	1.619091
8×8	0.321312	0.702915	0.960410	1.253279	1.578696
16×16	0.314811	0.690971	0.945723	1.235726	1.558095
32×32	0.313109	0.687847	0.941829	1.230899	1.552026
Analytical	0.322050	0.688258	0.933327	1.214635	1.531733

6.4 Geometrically nonlinear analysis of a clamped circular plate subjected to a uniform load

The large deformation analysis of a clamped circular plate subjected to a uniformly distributed load q is considered. The radius of the plate is $r = 100$ and the thickness of the plate is $h = 2$. The material properties are $E = 1.0e07$ and $\nu = 0.3$. The analytic central deflection w_0 of the plate is given by Chia (1980):

$$\frac{16}{3\left(1-\nu^2\right)}\left[\frac{w_0}{h} + \frac{1}{360}\left(1+\nu\right)\left(173-73\nu\right)\left(\frac{w_0}{h}\right)^3\right] = \frac{qr^4}{Eh^4} \tag{58}$$

Due to the double symmetry, only one quarter of the plate is discretized as shown in Fig.5. Fig.6 shows the comparison of the present result of the central deflection and the analytic solution by Chia (1980). It is observed that the present result is in very good agreement with the analytical solution.

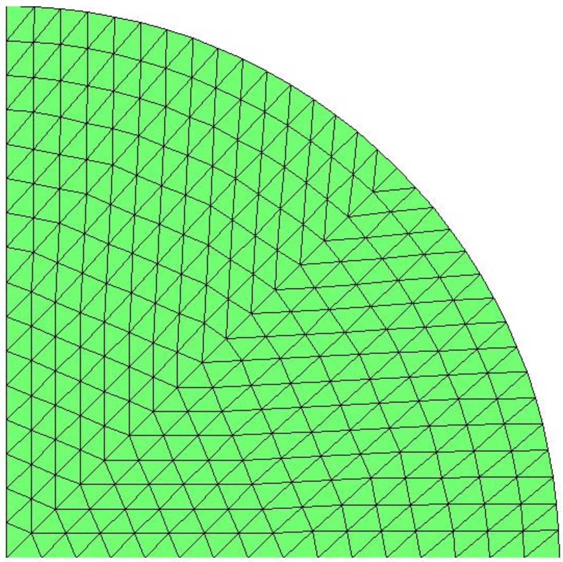

Figure 5: Mesh of one quarter of a clamped circular plate

6.5 Geometrically nonlinear analysis of a clamped circular plate subjected to a concentrated load

The circular plate subjected to a concentrated load p at the center of the plate is considered (Zhang and Cheung 2003). The geometric and material property are the same as the Section 5.4. Tab.5 gives the nondimensional central deflections w/h of the circular plate by using 289 nodes from the present method and the analytical solution by Chia (1980).

6.6 Nonlinear analysis of a cantilever plate with conservative end load

The cantilever plate with conservative end load shown in Fig.7 has been analyzed. The geometry parameters are $a = 40m$, $b = 30m$ and $h = 0.4m$. The material properties are $E = 1.2e8N/m^2$ and $\nu = 0.3$. The load-deflection curve is shown in Fig.8 where the present solution using a mesh of 8×8 is compared with the solution by

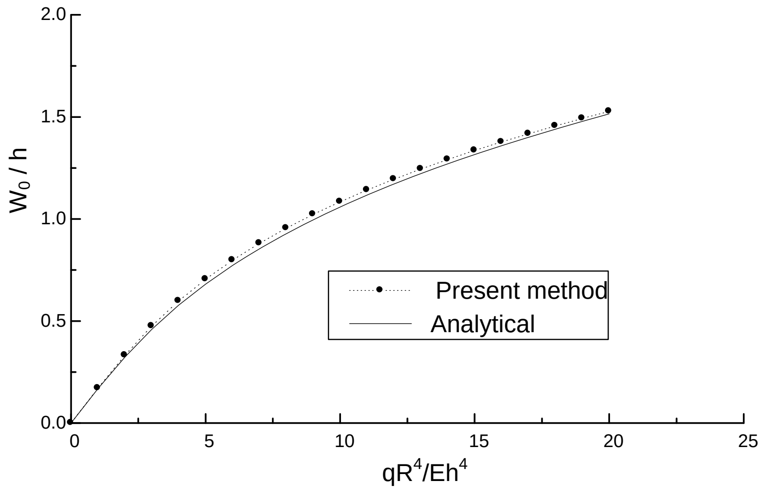

Figure 6: Nonlinear results of a clamped circular plate

Table 5: Nondimensional central deflection w/h of a clamped circular plate subjected to a concentrated load

	$pr^2/(Eh^4)$					
	1	2	3	4	5	6
Present method	0.2139	0.4080	0.5751	0.7182	0.8424	0.9520
Analytical solution	0.2129	0.4049	0.5695	0.7098	0.8309	0.9372

Oral and Barut (1991). W_A and W_B in Fig.8 are correspondingly the deflections of point A and point B along x_3.

6.7 Nonlinear analysis of a cylindrical shell panel

A cylindrical shell panel clamped along all four boundaries shown in Fig.9 is considered for nonlinear analysis. The shell panel is subjected to inward radial uniform load q. The geometry parameters are $l = 254mm$, $r = 2540mm$, $h = 3.175mm$ and $\theta = 0.1rad$. The material properties are $E = 3.10275kN/mm^2$ and $\nu = 0.3$. Due to the double symmetry, only one quarter of the panel is discretized using a mesh of 8×8. The present results of the central deflection together with solutions by Dhatt (1970) are shown in Fig.10. It is observed that the present method works very well.

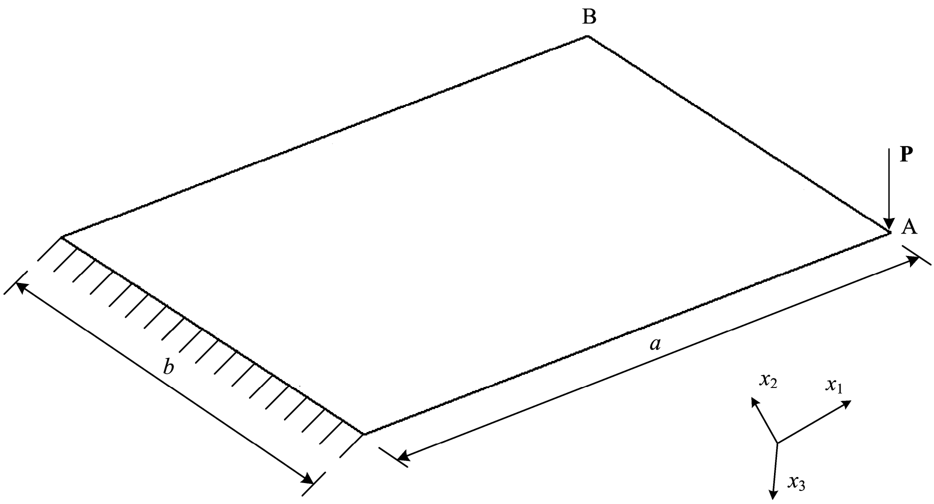

Figure 7: Cantilever plate with end load

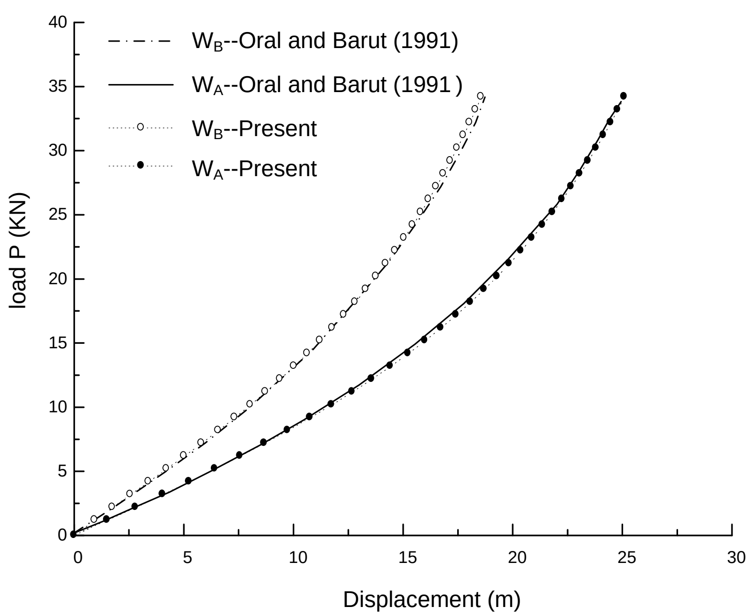

Figure 8: Load-deflection curve for the cantilever plate

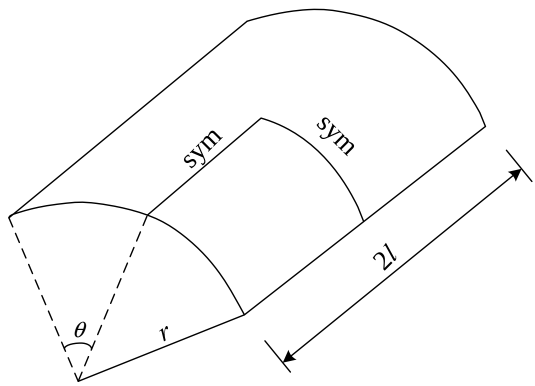

Figure 9: Model of the shell panel

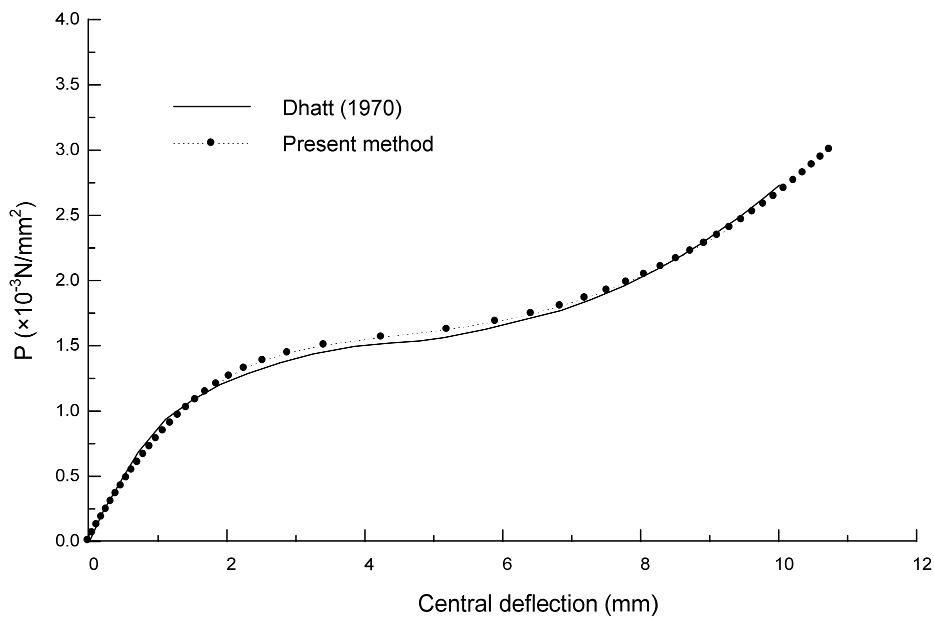

Figure 10: Nonlinear results of a clamped cylindrical shell panel

6.8 Hinged spherical shell with central point load

The hemispherical shell with an 18^0 hole shown in Fig.11 is analyzed. The geometry parameters are the radius $r = 10m$ and $h = 0.04m$. The material properties are $E = 6.825e7kN/m^2$ and $\nu = 0.3$. Due to the double symmetry, only one quarter of the shell is discretized using a mesh of 16×16(Fig.12). Fig.13 shows the present solutions based on primal method are in good agreement with the results of Kim and Lomboy (2006). The deformed shape of hemispherical shell with a mesh of 16×16 when $F = 200kN$ is shown in Fig.14.

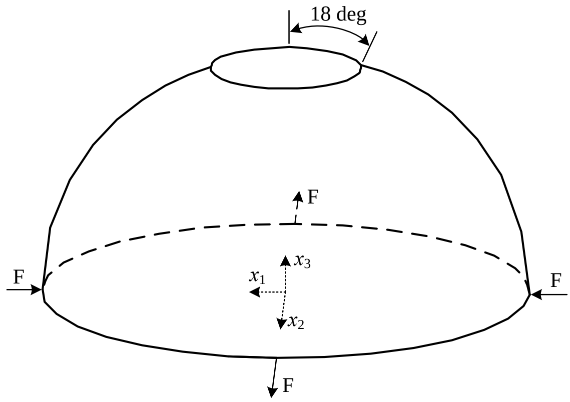

Figure 11: Model for hemispherical shell with an 18 ^{0} hole

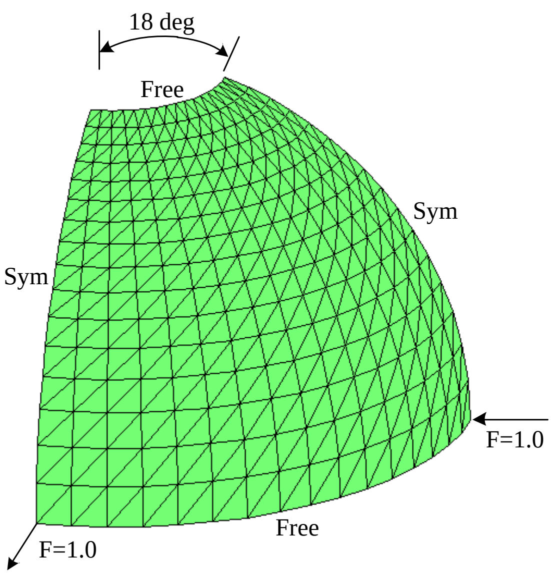

Figure 12: Mesh for the hemispherical shell with an 18 ^{0} hole

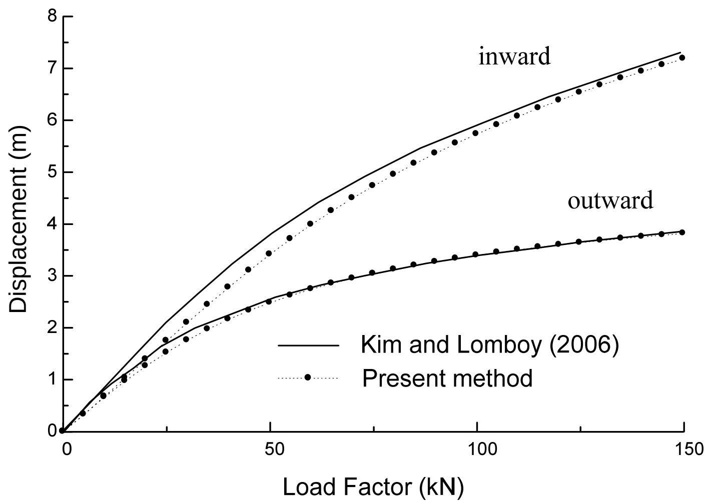

Figure 13: Nonlinear solutions for hemispherical shell

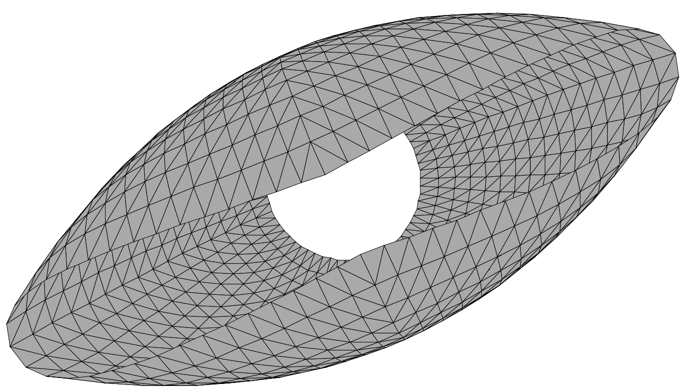

Figure 14: Deformed shape of hemispherical shell when $F = 200kN$

7 Conclusions

Based on a fully nonlinear theory of deformation in the co-rotational updated Lagrangian reference frame and the primal principle, a simple finite element method has been developed for large deformation/rotation analyses of plate/shell structures with thin members. It is shown to be possible to derive an explicit expression for the (18x18) symmetric tangent stiffness matrix of each element, including nodal displacements, nodal derivatives of transverse displacements, and nodal drilling degrees of freedom, even if assumed-displacement type formulations are used. The explicit expression and the numerical implementation of the present plate element are much simpler than many others in the literature for large rotation/deformation analysis of built-up plate/shell structures. While the present work is limited to elastic materials undergoing large deformations, the extension to inelasticity is straight forward and will be pursued in forthcoming publications.

Acknowledgement: The authors gratefully acknowledge the support of National Basic Research Program of China (973 Program: 2011CB013800), Program for Changjiang Scholars and Innovative Research Team in University (PCSIRT, IRT1029), and Fundamental Research Funds for the Central Universities (Tongji university). This research was also supported in part by an agreement of UCI with ARL with D.Le, M.Haile and A.Ghoshal as cognizant collaborators, and by the World Class University (WCU) program through the National Research Foundation of Korea funded by the Ministry of Education, Science and Technology (Grant no.: R33-10049).

References

Albuquerque, E.L.; Aliabadi, M.H. (2008): A boundary element formulation for boundary only analysis of thin shallow shells. *CMES:Computer Modeling in Engineering & Sciences*, Vol.29, pp.63-73.

Atluri, S.N. (1980): On some new general and complementary energy theorems for the rate problems in finite strain, classical elastoplasticity. *Journal of Structural Mechanics*, Vol. 8(1), pp. 61-92.

Atluri, S.N. (2005): Methods of Computer Modeling in Engineering & Science. Tech Science Press.

Atluri, S.N.; Cazzani, A. (1994): Rotations in computational solid mechanics, invited feature article. *Archives for Computational Methods in Engg.*, ICNME, Barcelona, Spain, Vol 2(1), pp. 49-138.

Baiz, P.M.; Aliabadi, M.H. (2006): Linear buckling analysis of shear deformable shallow shells by the boundary domain element method. *CMES:Computer Modeling in Engineering & Sciences*, vol.13, pp.19-34.

Cai, Y.C.; Paik, J.K.; Atluri S.N. (2010): A triangular plate element with drilling degrees of freedom, for large rotation analyses of built-up plate/shell structures, based on the Reissner variational principle and the von Karman nonlinear theory in the co-rotational reference frame. *CMES: Computer Modeling in Engineering & Sciences*, vol. 61, pp.273-312

Chia, C.Y. (1980): Nonlinear Analysis of Plate. McGraw-Hill, New York.

Chin,Y.;Zhang, J.Y. (1994): A new hybrid quadrilateral finite element for Mindlin plate. *Applied Mathematics and Mechanics*, Vol.15, pp. 189-199.

Choo, Y.S.; Choi, N.; Lee, B.C.(2010): A new hybrid-Trefftz triangular and quadrilateral plate elements. *Applied Mathematical Modelling*, Vol. 34, pp. 14-23.

Dhatt, G.S. (1970): Instability of thin shells by the finite element method. IASS Symposium for Folded Plates and Prismatic Structures, Vienna.

Fedelinski, P.; Gorski, R. (2006): Analysis and optimization of dynamically loaded reinforced plates by the coupled boundary and finite element method. *CMES: Computer Modeling in Engineering & Sciences*, Vol.15, pp.31-40.

Gal, E.; Levy, R. (2006): Geometrically nonlinear analysis of shell structures using a flat triangular shell finite element. *Arch. Comput. Meth. Engng.*, Vol. 13, pp. 331-388.

Huang, B.Z.; Shenoy, V.B.; Atluri, S.N. (1994): A quasi-comforming triangular laminated composite shell element based on a refined first-order theory. *Computational Mechanics*, Vol.13, pp.295-314.

Iura, M.; Atluri, S.N. (1992): Formulation of a membrane finite element with drilling degrees of freedom. *Computational Mechanics*, Vol.9, pp.417-428.

Iura, M.; Atluri, S.N. (2003): Advances in finite rotations in structural mechanics. *CMES:Computer Modeling in Engineering & Sciences*, Vol.4, pp.213-215.

Kang, L.; Zhang, Q.L.; Wang, Z.Q. (2009): Linear and geometrically nonlinear analysis of novel flat shell elements with rotational degrees of freedom. *Finite Elements in Analysis and Design*, Vol.45,pp.386–392.

Kim, K.D.; Lomboy, G.R. (2006): A co-rotational quasi-conforming 4-node resultant shell element for large deformation elasto-plastic analysis .*Computer Methods in Applied Mechanics and Engineering*, vol.195, pp. 6502-6522.

Kulikov, G.M.; Plotnikova, S.V. (2008): Finite rotation geometrically exact four-node solid-shell element with seven displacement degrees of freedom. *CMES: Computer Modeling in Engineering & Sciences*, Vol.28, pp. 15-38.

Maunder, E.A.W.; Moitinho, J.P. (2005):A triangular hybrid equilibrium plate element of general degree. *International Journal for Numerical Methods in Engineering*, Vol.63, pp. 315-350.

Nguyen-Van, H.; Mai-Duy, N.; Tran-Cong, T. (2007): A simple and accurate four-node quadrilateral element using stabilized nodal integration for laminated plates. *CMC:Computers Materials & Continua*, vol.6, pp.159-175.

Oral, S.; Barut, A. (1991): A shear-flexible facet shell element for large deflection and instability analysis. *Computer Methods in Applied Mechanics and Engineer-*

ing, vol. 93, pp. 415-431.

Rajendran, R.; Narasimhan, K. (2006): Deformation and fracture behaviour of plate specimens subjected to underwater explosion - a review. *International Journal of Impact Engineering*, Vol.32, pp.1945-1963.

Wu, C.P.; Chiu, K.H.; Wang, Y.M. (2008): A review on the three-dimensional analytical approaches of multilayered and functionally graded piezoelectric plates and shells. *CMC:Computers Materials & Continua*, Vol.8, pp.93-132.

Zhang, Y.X.; Cheung, Y.K. (2003): Geometric nonlinear analysis of thin plates by a refined nonlinear non-conforming triangular plate element. *Thin-Walled Structures*, Vol.41, pp.403-418.